A Knowledge-based Approach to Urban Feature Classification Using Aerial Imagery with Lidar Data

Ming-Jer Huang, Shiahn-Wern Shyue, Liang-Hwei Lee, and Chih-Chung Kao

Abstract

While the spatial resolution of remotely sensed data has improved, multispectral imagery is still not sufficient for urban classification. Problems include the difficulty in discriminating between trees and grass, the misclassification of buildings due to diverse roof compositions and shadow effects, and the misclassification of cars on roads. Recently, lidar (light detection and ranging) data have been integrated with remotely sensed data to obtain better classification results. In this study, we first conducted maximum likelihood classification (MLC) experiments, a traditional pixel-based classification method, to identify features suitable for urban classification using lidar data and aerial imagery. The addition of lidar height data improved the overall accuracy by up to 28 and 18 percent, respectively, compared to cases with only red–green–blue (RGB) and multispectral imagery. To further improve classification, we propose a knowledge-based classification system (KBCS) that includes a three-level height, "asphalt road, vegetation, and non-vegetation" (A–V–N) classification rule-based scheme and knowledge-based correction (KBC). The proposed KBCS improved overall accuracy by 12 and 7 percent compared to maximum likelihood and object-based classification, respectively.

Introduction

Remotely sensed data from airborne and spaceborne platforms offer global coverage at varying spatial, spectral, and temporal resolutions, and are the major source of geospatial information (Baltsavias and Gruen, 2003). Among data sources, aerial/satellite imagery with multispectral bands is widely used to investigate natural resources and classify land-use and land-cover. The red edge between the red and near infrared (NIR) bands can effectively discriminate vegetation and other land-cover. However, while the image information content increases with spatial resolution, the accuracy of land-cover classification may actually decrease, a problem that cannot be overcome by a traditional pixel-based approach. Recently, classification technology has progressed from traditional pixel-based statistical methods to knowledge- and object-based classification (OBC) approaches (Hodgson *et al.*, 2003; Taubenböck *et al.*, 2006).

However, a common criticism of OBC is that the analyst must have sufficient knowledge about the land-cover objects in individual images. The analyst then applies this knowledge to construct a hierarchical image object network by using iterative procedures to find the optimal segmentation parameters for classification. The segmentation parameters applied by the analyst will influence the classification results (Baatz *et al.*, 2004; Repake *et al.*, 2004). The adoption of expert systems or knowledge-based classification methods may improve not only OBC performance but also classification accuracy from multisource remote sensing data (Richards and Jia, 1999). Early research demonstrated the application of knowledge-based techniques to remotely sensed data (Nagao and Matsuyama, 1980). These techniques have since been applied to urban land-cover discrimination using Landsat TM imagery (Ton *et al.*, 1991). They have also been integrated with multiple classification methods to improve classification accuracy (Liu *et al.*, 2002; Stefanov *et al.*, 2001) and combined with expert rules in a sub-pixel MLC classifier as part of a vegetation-impervious surface-soil (V–I–S) conceptual model to successfully model an urban ecosystem (Hung and Ridd, 2002).

The goal of classification is to effectively discriminate ground features. While the horizontal information for categories, shapes, and boundaries of ground features can be determined, urban features are so complex that multispectral imagery and traditional classification techniques are not sufficient for classifying them. For example, while it is generally easy to distinguish vegetation and man-made objects using NIR images, it is still very difficult to discriminate between trees and grass. Moreover, buildings may be classified into other categories because of spectral variations caused by apparent differences in roof composition and shadow effects. However, such misclassification may be resolved by adding height information. Therefore, even withot NIR, using color images (containing only RGB bands) together with lidar (light detection and ranging) data may improve classification accuracy.

Ming-Jer Huang and Shiahn-Wern Shyue are with the Department of Marine Environment and Engineering, Asian Pacific Ocean Research Center, National Sun Yat-Sen University, 70 Lien-hai Road, Kaohsiung 804, Taiwan ROC (swshyue@faculty.nsysu.edu.tw).

Liang-Hwei Lee is with the Department of Civil Engineering, National Kao-Hsiung University of Applied Sciences, 415 Chien Kung Road, Kaohsiung 80778, Taiwan, ROC.

Chih-Chung Kao is with the Department of Information Management, Fortune Institute of Technology, 14FL, 62 Chien-An Street, San-Min District, Kaohsiung, Taiwan, R.O.C.

Photogrammetric Engineering & Remote Sensing
Vol. 74, No. 12, December 2008, pp. 1473–1485.

0099-1112/08/7412–1473/$3.00/0

Lidar integrates a global positioning system (GPS) device, inertial motion unit (IMU), and laser scanner to create high-resolution and accurate digital surface models (DSMs). Lidar-derived normalized DSMs (NDSMs) provide useful information for urban building extraction (Haala and Brenner, 1999; Rottensteiner *et al.*, 2005), and urban land-use classification (Hill *et al.*, 2002; Hodgson *et al.*, 2003). The studies noted above have suggested that the integration of aerial images and lidar-derived NDSMs may hold great potential for urban classification (Rottensteiner *et al.*, 2005). However, those studies either only compared the contribution of NDSMs to classification visually (Haala and Brenner, 1999) or investigated the relative contribution of NDSMs to imperviousness modeling (Hodgson *et al.*, 2003). Therefore, quantitative as well as qualitative evaluation of the contribution to urban classification of adding lidar NDSMs and intensity to color or multispectral aerial imagery data is needed.

New types of digital aerial cameras, such as the digital mapping camera (DMC) or ADS40 camera, provide RGB as well as NIR images (Baltsavias and Gruen, 2003). Many manufacturers are also now producing highly efficient lidar systems, and the data provided are expected to greatly improve classification performance. However, determining the optimal features for urban classification is a critical task. This study had two objectives with the aim of achieving this goal. First, we investigated the feasibility and contribution of lidar data integrated with high-resolution color aerial imagery and NIR band imagery in regard to urban classification. Second, to further improve classification performance, a knowledge-based classification system (KBCS) was developed. The developed knowledge base includes road-, vegetation-, and building-discrimination rules based on the characteristics of remotely sensed data and expert knowledge. A three-height-level, rule-based classification framework according to a lidar NDSM was established. In each level, the "asphalt road, vegetation, and non-vegetation" (A–V–N) classification principle was used to simplify the categories. Next, knowledge-based correction (KBC) was applied to adjust for some misclassification. This paper describes the algorithms, the knowledge-base construction procedures, and the organization of the proposed methodology. Experimental results are presented to demonstrate the benefits of the integration of aerial imagery with lidar data as well as the greater classification accuracy of the proposed KBCS compared with the OBC approach.

Construction of the Knowledge Base

Although various ways of expressing expert knowledge exist, rules are the most common and simplest way to create a knowledge-based system (Giarratano and Riley, 1989). The rules are given in the form of "if < condition > then < conclusion >." Each rule represents one item of knowledge captured from remotely sensed data associated with a threshold that is either assigned by experts or calculated automatically according to the characteristics of the ground feature. In addition to the thresholds used by data-driven rules, a logical threshold is used to help decide whether a specific rule is applied. Table 1 lists all the thresholds used

TABLE 1. THRESHOLD VALUES AND SWITCHES LOGICAL THRESHOLD

Thresholds			Value Used	
NO	Threshold Name	Explanation	Study Area 1	Study Area 2
1	$Threshold_{HL}$	Low height level height	0.5 m	0.5 m
2	$Threshold_{HH}$	High height level height	2.5 m	2.0 m
3	$Threshold_{IL}$	Low lidar intensity	5	5
4	$Threshold_{IH}$	High lidar intensity	18	15
5	$Threshold_{Smoothness}$	Smoothness threshold	3.0 m	3.0 m
6	$Threshold_{Penetrability}$	Penetrability threshold	0.05 m	0.05 m
7	$Threshold_{LBA}$	Smallest Building Block Area	1800 p	1800 p
8	$Threshold_{ShapeIndex}$	Shape Index	0.5	0.5
9	$Threshold_{Area}$	Smallest Area	225 p	225 p
10	$Threshold_{TVI}$	lidar-TVI	Automatic	Automatic
11	$Threshold_{NDVI}$	NDVI	Automatic	Automatic
12	$Threshold_{43}$	Remove grass from roads	1250	1250
13	$Threshold_{34}$	Remove roads from grass	750	750
14	$Threshold_{21}$	Remove trees from buildings	750	750
15	$Threshold_{12}$	Remove buildings from trees	750	750
16	$Threshold_{31}$	Remove roads from buildings	1500	1500
17	$Threshold_{41}$	Remove grass from buildings	1500	1500
18	$Threshold_{32}$	Remove roads from trees	0	750

Notes:
Threshold 1~9: Input by user. The values in parenthesis are default values (p: pixels).
Threshold 10, 11: Automatic means calculated by automatic optimum threshold selection method.
Threshold 12–18: When the threshold is greater than 0, this function is activated.

Logical Thresholds		Value Used	
NO	Threshold Name	Study Area 1	Study Area 2
1	Use_NDVI_for_Trees	Y	Y
2	Use_NDVI_for_Grass	Y	Y
3	Use_LIDAR-TVI_for_Grass	Y	Y
4	Use_LIDAR-TVI_for_Trees	N	Y
5	Use_ND_for_Trees	N	Y
	Use_AIS_for_Trees	N	Y
6	Use_Penetrability_for_Grass	N	N
7	Use_Mask	Y	N

in this work. Several recent studies have explored urban-feature extraction from aerial imagery and lidar data by focusing on three major categories: roads, vegetation, and buildings. Good results have been obtained from individual studies (Arefi *et al.*, 2003; Elberink and Mass, 2000; Haala and Brenner, 1999; Hu and Tao, 2005; Ma, 2005). However, to establish discriminative models and a knowledge-acquisition procedure, these accumulated research results must be adjusted according the characteristics of the study area and the data. The following sections discuss the decision process behind each of the three feature-discrimination models, the types of data needed, and the method of obtaining optimal thresholds to segment the feature images for classification.

Prior Knowledge Rules

Three Level Height Rules (Rules P1 to P3)

Three height levels were established for the lidar NDSM by selecting two height thresholds ($Threshold_{HL}$ and $Threshold_{HH}$). The first threshold was defined by a very low height value (e.g., 0.5 m), and the other was defined according to the lowest building height (e.g., 2.5 m) in each different study area. The rules that define the three levels (Rules P1 to P3) can be written as:

$$\begin{aligned}&\textbf{If } nDSM < Threshold_{HL} \textbf{ then } low\_height = true\\ &\textbf{If } nDSM >= Threshold_{HL} \textbf{ and } nDSM < Threshold_{HH}\\ &\textbf{then } mid\_height = true\\ &\textbf{If } nDSM >= Threshold_{HH} \textbf{ then } high\_height = true.\end{aligned} \quad (1)$$

Area Analysis Rule (Rule P4)

Generally, in image segmentation, a great deal of noise may remain after applying a specific type of knowledge to extract objects that meet a criterion. If the total pixels of a connected component are smaller than a threshold, that component will be treated as noise. For an image with a 0.1 m spatial resolution, the threshold of 225 pixels represents an area of about 1.5 m × 1.5 m. The Area Analysis Rule can be applied to all of the following discriminative models and written as:

$$\textbf{If } Area(X) < Threshold_{Area} \textbf{ then } X = false,$$

where X is the derived segment image from a specific rule.

Road Discriminative Model (RDM)

Lidar Intensity Road Rule (Rule R1)

Examination of the pixel values from the lidar intensity image shows that high values appear over grass, vehicles, and lane markings on roads. In contrast, asphalt roads usually have low lidar intensity compared to other objects. The Lidar Intensity Road Rule (Rule R1) can be derived by setting up two lidar intensity thresholds ($Threshold_{IL}$ and $Threshold_{IH}$) to extract asphalt roads. This rule can be written as:

$$\begin{aligned}&\textbf{If } LidarIntensity > Threshold_{IL} \textbf{ and}\\ &\quad LidarIntensity < Threshold_{IH}\\ &\textbf{then } Road = true.\end{aligned}$$

However, the detected asphalt road image contains excess noise coming from objects with high lidar intensity values. As a result, the road discriminative models require more rules based on lidar height to identify other road characteristics.

Smoothness Road Rule (Rule R2)

The second road discriminative rule is based on the characteristic of road surfaces in urban areas to be relatively smooth. Under this condition, the smoothness can be defined by calculating the height difference between a lidar point and a locally planar surface. Height differences of less than a threshold are classified as points on smooth surfaces, such as roads or building roofs (Ma, 2005). Ma (2005) suggested 0.3 m as the threshold for smooth surface determination. According to our experiment results, this threshold can correctly classify most planar points. The Smoothness Road Rule (Rule R2) can be written as:

$$\textbf{If } Smoothness < Threshold_{Smoothness} \textbf{ then } Road = true.$$

Penetrability Road Rule (Rule R3)

The third road discriminative rule is described by penetrability, which is defined by how well the laser beam from the lidar system can penetrate through objects, such as trees, to the ground. Roads have low penetrability. To describe low-penetrability roads, the lidar height difference between first return ($H_{First\ Return}$) and last return ($H_{Last\ Return}$) is close to zero (e.g., 0.05 m). This rule can be written as:

$$\textbf{If abs } (H_{First} - H_{Last}) < Threshold_{Penetrability} \textbf{ then } Road = true.$$

Integrated Vegetation Discriminative Model (IVDM)

This study proposes an Integrated Vegetation Discriminative Model (IVDM) based on previous research results with some modifications to enhance the capability to separate ground objects and define them as vegetation or non-vegetation (Arefi *et al.*, 2003; Elberink and Mass, 2000; Huang *et al.*, 2006; Ma, 2005;).

NDVI Vegetation Rules (Rules V1 and V2)

The normalized difference vegetation index (NDVI) is generally used to discriminate vegetation from other land-cover. We used Otsu's (1979) method to compute the threshold ($Threshold_{NDVI}$) for the NDVI vegetation rule. Because the NIR band of aerial imagery is not always available, the rules used for tree and grass discrimination must be accompanied by a logical threshold. The NDVI Tree Rule (Rule V1) can be written as:

$$\begin{aligned}&\textbf{If } Use\_NDVI\_for\_Trees = true \textbf{ and } NDVI > Threshold_{NDVI}\\ &\textbf{then } Tree = true.\end{aligned}$$

Because most grass in urban areas is lawn, the NDVI Grass Rule must be used together with the low penetrability rule. Otherwise, the NDVI Grass Rule is identical to the NDVI Tree Rule. The NDVI Grass Rule (Rule V2) can be written as:

$$\begin{aligned}&\textbf{If } Use\_NDVI\_for\_Grass = true \textbf{ and}\\ &\quad NDVI > Threshold_{\mathrm{NDVI}} \textbf{ and abs}\\ &\quad (\mathrm{H_{First}}–\mathrm{H_{Last}}) < Threshold_{Penetrability}\\ &\textbf{then } Grass = true.\end{aligned}$$

Lidar-TVI Vegetation Rule (Rules V3 and V4)

The transformed vegetation index (TVI) modifies the NDVI by adding a constant of 0.50 to all NDVI values and taking the square root of the results (Deering *et al.*, 1975). In this study, we apply a Lidar–TVI, which replaces the NIR band with lidar intensity in the TVI formula (Huang *et al.*, 2006), as follows:

$$Lidar–TVI = \sqrt{\frac{(Lidar\ Intensity - RED)}{(Lidar\ Intensity + RED)} + 0.5}. \quad (2)$$

The derived Lidar-TVI Vegetation Rule also uses Otsu's (1979) method to calculate the threshold. The Lidar-TVI Grass Rule (Rule V3) can be written as:

$$\begin{aligned}&\textbf{If } Use\_Lidar\_TVI\_for\_Grass = true \textbf{ and}\\ &\quad Lidar–TVI > Threshod_{TVI}\\ &\textbf{then } Grass = true.\end{aligned}$$

Huang *et al.* (2006) concluded that Lidar–TVI performs well for grass discrimination but misses some trees due to low-intensity values. However, when the NDVI is insufficient to extract trees, Lidar–TVI is an option for tree discrimination. The Lidar–TVI Tree Rule can be written as:

If *Use_Lidar_TVI_for_Tree = true* **and**
Lidar–TVI $>$ *Threshod*$_{TVI}$
then *Tree = true.*

ND Tree Rule (Rule V5)
Normalized difference (ND) is a lidar-based vegetation index calculated by the difference between the lidar height of the first return (H_{First}) and the last return (H_{Last}). The equation for ND is defined as (Arefi *et al.*, 2003):

$$ND = \frac{(H_{First} - H_{Last})}{(H_{First} + H_{Last})}. \quad (3)$$

Because large lidar height differences due to multiple returns may also occur at the boundaries of buildings in a ND image, the following procedure should be performed to remove these high values. First, pixels with a height gradient greater than a threshold value should be eliminated. According to our experiments, a threshold value between 1 and 1.25 can remove most of the building boundaries in a ND image. Next, Otsu's (1979) automatic threshold selection method is used to find the optimum threshold for extracting trees from ND images. Finally, morphological erosion and connected component area filtering are applied to clean up the noise. The morphological dilation process should be performed on the resultant image one pixel outward after morphological erosion. The postprocessed segmentation image of the ND is then used as the basis of the ND Tree Rule (Rule V5), written as:

If *ND = true* **then** *Tree = true.*

However, the ND Tree Rule is not capable of finding dense trees because the lidar laser beam cannot penetrate through dense trees to the ground, especially at the center of large trees. Therefore, we need the AIS Tree Rule to enhance the tree-extraction capability of the KBCS.

AIS Tree Rule (Rule V6)
The Anisotropic Smoothness (AIS) Tree Rule, the second lidar-based vegetation index, integrates the smoothness filter proposed by Ma (2005) and the anisotropic operator proposed by Elberink and Mass (2000). Two major ground features with non-flat characteristics in the AIS resultant image are trees and building boundaries. The same post-processing procedure used for removing building boundaries for ND calculation is also applied to remove building boundaries in the AIS binary image. The AIS Tree Rule can be written as:

If *AIS = true* **then** *Tree = true.*

Building Correction Rules (Rule B1 and Rule B2)

In urban areas, rooftops may contain several complex human-made structures. It is difficult to find a universal pattern for a building discriminative model. We propose two building correction rules to exclude such non-building objects. First, each connected component in the high-height level (the connected buildings surrounded by streets) with an area less than a threshold ($Threshold_{Area}$) is eliminated. Second, the shape index, defined by the ratio of the perimeter to the area of the building block, is used to remove narrow and long connected components that have shape index values below a threshold ($Threshold_{ShapeIndex}$). Our experiments indicate that a threshold of 0.5 can remove most narrow and long buildings. The building correction rules (Rules B1 and B2) can be written as:

If *Area(X)* $<$ *Threshold*$_{Area}$ **then** *building = false*
If *ShapeIndex* $<$ *Threshold*$_{ShapeIndex}$ **then**
building = false.

Table 2 lists all the rules used in this study: the four prior knowledge rules (Rules P1 to P4), three road rules (Rules R1 to R3), six vegetation rules (Rules V1 to V6), and two building correction rules (Rules B1 and B2). These rules can be combined with the thresholds in Table 1 and formalized as an intensive knowledge base.

Three Level Rule-based Classification

Three Level Selection and Definition

This study proposes a new three-height-level, rule-based classification scheme of low-, mid-, and high-height levels. The low-height level, defined by a very low height value (e.g., 0.5 m), extracts objects near the ground, while the high-height level is defined according to the lowest building height (e.g., 2.5 m) in the study area. Correspondingly, objects in between the two height thresholds can be discriminated at the mid-height level. The mid-height level is included for correct classification at this level and to increase classification accuracy. Objects at this level, such as cars, traffic control boxes, and telephone booths may not be large or permanent fixtures and do not have a consistent pattern for classification. These ground objects are separated before classification, consequently reducing the number of categories at each level.

This scheme clarifies the importance and functionality of lidar height in a classification system from a new viewpoint. Lidar height is not only used for texture in the classification system, but also divides the vertical dimension into three stratification levels and then extracts ground-feature segments from each level. This unique scheme is not found in traditional pixel-based classification, and the OBC approach uses lidar height data only to represent objects horizontally without considering the vertical direction. Each level uses a segment-based classification scheme. These classified segments derived from applying the rules are combined as the classification results of each level. The classified result from one level lower than the current level is then aggregated to the current level. This specially designed scheme, as shown in Figure 1, is a knowledge-based, segment-based, vertical stratification; a rule-based classification; and an aggregation scheme.

A–V–N Classification Principle

Theoretically, no accessing order exists for applying rules in a KBCS. Nevertheless, to overcome the complexity of urban-feature classification, we set up an A–V–N classification principle to prioritize the application of rules in the knowledge base. This principle can simplify the wide variety in the heterogeneous urban environment into a combination of four major categories (buildings, trees, roads, and grass) for construction of the cyber city. This simplification is related to the V–I–S conceptual model proposed by Hung and Ridd (2002) and Ridd (1995).

The objects at the low-height level are mainly roads and grass, and most grass in urban areas is lawn. Moreover, lawn grass and roads generally have very low penetrability, which makes the separation of grass from roads difficult based on lidar height, and because the lidar intensity over grass, cars, or lane markings on roads is high, it becomes

TABLE 2. RULES

Category	Rule Name	Rule ID	Rule Definition
Prior Knowledge Rules	Low-Height Level Rule	Rule P1	**If** $nDSM < Threshold_{HL}$ **then** *low_height = true*
	Mid-Height Level Rule	Rule P2	**If** $nDSM >= Threshold_{HL}$ **and** $nDSM < Threshold_{HH}$ **then** *mid_height = true*
	High-Height Level Rule	Rule P3	**If** $nDSM >= Threshold_{HH}$ **then** *high_height* = true
	Area Analysis Rule	Rule P4	**If** $Area(X) < Threshold_{Area}$ **then** *X = false*
Road Rules	LIDAR Intensity Road Rule	Rule R1	**If** $LidarIntensity > Threshold_{IL}$ **and** $LidarIntensity < Threshold_{IH}$ **then** *Road = true*
	Smoothness Road Rule	Rule R2	**If** $Smoothness < Threshold_{Smoothness}$ **then** *Road = true*
	Penetrability Road Rule	Rule R3	**If** $\mathbf{abs}(H_{First}-H_{Last}) < Threshold_{Penetrability}$ **then** *Road = true*
Vegetation Rules	NDVI Tree Rule	Rule V1	**If** *Use_NDVI_for_Trees = true* **and** $NDVI > Threshold_{NDVI}$ **then** *Tree = true*
	NDVI Grass Rule	Rule V2	**If** *Use_NDVI_for_Trees = true* **and** $NDVI > Threshold_{NDVI}$ **and** $\mathbf{abs}(H_{First}-H_{Last}) < Threshold_{Penetrability}$ **then** *Grass = true*
	LIDAR-TVI Grass Rule	Rule V3	**If** *Use_LIDAR-TVI_for_Grass = true* **and** $LIDAR\text{-}TVI > Threshold_{TVI}$ **then** *Grass = true*
	LIDAR-TVI Tree Rule	Rule V4	**If** *Use_LIDAR-TVI_for_Trees = true* **and** $LIDAR\text{-}TVI > Threshold_{TVI}$ **then** *Tree = true*
	ND Tree Rule	Rule V5	**If** *ND = true* **then** *Tree = true*
	AIS Tree Rule	Rule V6	**If** *AIS = true* **then** *Tree = true*
Building Rules	Building Area Correction Rule	Rule B1	**If** $Area(X) < Threshold_{Area}$ **then** *Building = false*
	Building Shape Correction Rule	Rule B2	**If** $ShapeIndex < Threshold_{ShapeIndex}$ **then** *Building = false*

very easy to confuse grass and roads. However, the lidar intensity over asphalt roads is relatively low. Therefore, the following strategy can be used for applying classification rules in this level: first separate the asphalt roads using the Lidar Intensity Road Rule; next, discriminate the vegetation by using the IVDM, and then extract the non-vegetation. This procedure conforms to the proposed A–V–N classification principle.

At the mid-height level, asphalt roads may overlap with mobile objects, such as cars, or stationary objects such as traffic control boxes and telephone booths. These ground objects must be modeled in a way that compensates for the spatial incoherence of roads. In this study, because our aim is cyber city modeling, these small mobile objects were intentionally merged into the road category. Other than roads and grass, vegetation at this level may include shrubs, grassy field areas, or raised planting beds in parks. The strategy of applying the classification rules at this level still obeys the A–V–N classification principle.

The two main categories of ground objects at the high-height level are buildings and trees. Even though asphalt roads do not occur at this level, the A–V–N classification principle is still valid in resolving the complexity between buildings and trees. The classification strategy at this level is to first extract the trees using the rules of the IVDM and then to separate the buildings using the building correction rules.

Knowledge-based Correction (KBC)

The KBC procedures are conducted in two stages. First, residual reposition is performed after applying rule-based classification at each level. To fulfill the characteristics of spatial coherence, small segments removed by the Area Analysis Rule (Rule P4), the residuals of that specific level, can be reassigned to a neighboring ground feature type if they are next to a specified ground feature appointed by the rule in the knowledge base. After completing the three-level rule-based classification, the second stage of KBC, temporal adjustment, ground-feature generalization, and shape index analysis are performed to adjust the classification results.

For a growing city, changes may be ongoing and occurring rapidly. Therefore, in a multisource classification application, data sources acquired at different times may show temporal inconsistencies. The procedure to adjust temporal inconsistency involves temporal mask construction and class adjustment. First, a temporal mask is defined by a manually digitized boundary vector file and a feature layer. Pixels within the boundary are all assigned true values. An image containing all true values is created as a boundary mask to specify where the change

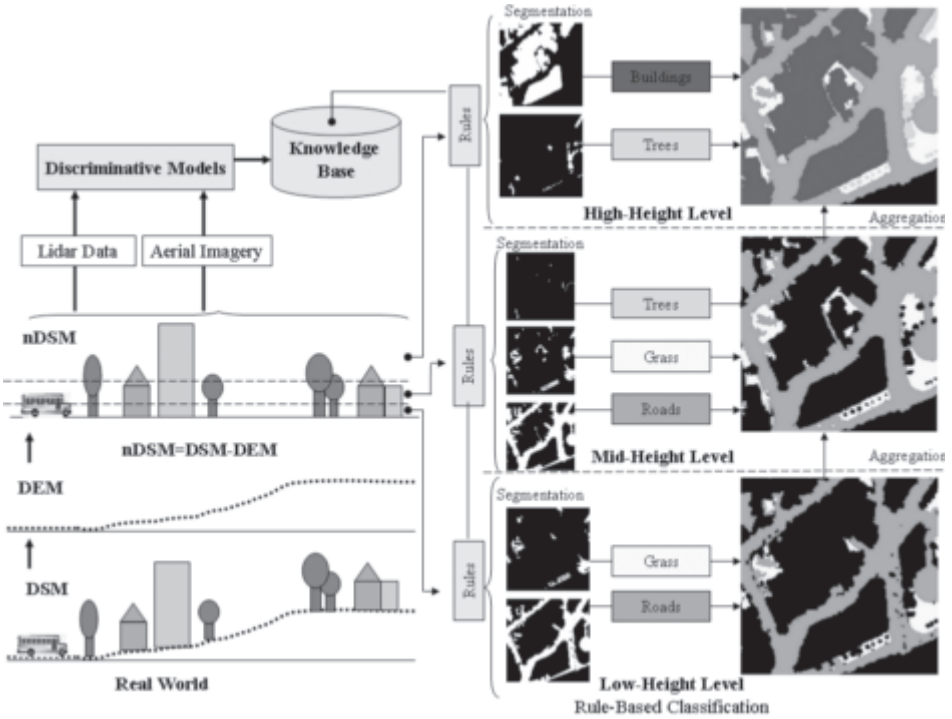

Figure 1. Knowledge- and segment-based vertical stratification, rule-based classification, and aggregation schemes. A color version of this figure is available at the ASPRS website: **www.asprs.org**.

occurs. Next, automatic recognition of the change area within the boundary mask is used to check the pixel brightness values according to specific criteria. Pixels that match the criteria and occur within the boundary mask are used to create the temporal mask. Afterwards, any class within the defined temporal mask is adjusted to a new class as specified in the temporal adjusting rules defined by the user according to the real changes observed in the updated imagery.

The purpose of ground-feature generalization is to combine small segments into meaningful categories. These small image segments can be observed from the initial knowledge-based classification results. For example, cars on roads, potted plants on building roofs, and traffic lights and traffic control boxes on roads are all within the mid-height level. These features are visible due to the spectral and spatial heterogeneity of high-resolution imagery and lidar data, and are neither noise nor errors due to classification. However, these features should sometimes be intentionally ignored, depending on the level of detail required for urban-feature classification. The ground-feature generalization checks each of the classified small segments having area less than a threshold, and determines whether its feature type is surrounded by another ground-feature type. If so, this small segment will be merged into the surrounding segments with the same ground-feature type. Table 1 lists these adjustment thresholds.

Shadows caused by buildings should also be handled at this point. Most building blocks cast long and narrow shadows; therefore, shape index analysis can be applied to remove these shadow features of the segments. Long and narrow shape segments with a shape index between 0.5 and 0.8 are categorized as non-buildings based on our experiments.

KBCS Implementation

A major advantage of the KBCS is that we can use the experience and knowledge from previous studies to construct a knowledge base for urban-features extraction. Figure 2 shows the workflow of the proposed KBCS. First, the knowledge base is constructed by the knowledge-acquisition procedure from aerial imagery and lidar data. Next, the three-level, rule-based classification is performed according to the rules of the knowledge base. Afterward, the classification result is adjusted by the KBC module. Finally, the KBCS classifies the aerial imagery into four major urban categories. In this study, Matlab was used to implement the KBCS according to the methodology described above. The KBCS output was stored in ENVI native image format and assessed for accuracy.

Experiments

Study Areas and Data Sets

The study site, Kaohsiung City, a harbor city with a long history of development, is located in the southwestern part of Taiwan (Figure 3). This area is a mix of apartment buildings, small lanes, industry facilities, and a world-class harbor. Two study areas including two different types of urban features were selected. Study area 1 is an urban area with many small and large buildings, larger-sized buildings, a big parking lot, and a grassy field. Figure 4 shows the aerial imagery and lidar height image of this area. Study area 2 is on an island across the harbor from study area 1. This area is not level and instead slopes down to the harbor. A large park with dense trees is on the seaward side of the island. This area also features a mixture of variously sized buildings, as shown in Figure 5.

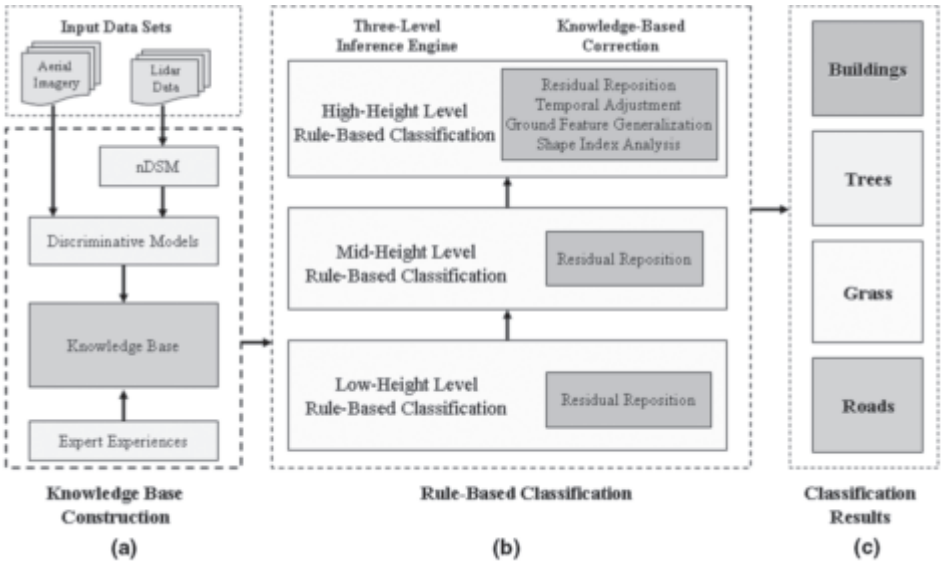

Figure 2. Workflow of the KBCS: (a) Knowledge Base Construction, (b) Rule-based Classification, and (c) Classification Results.

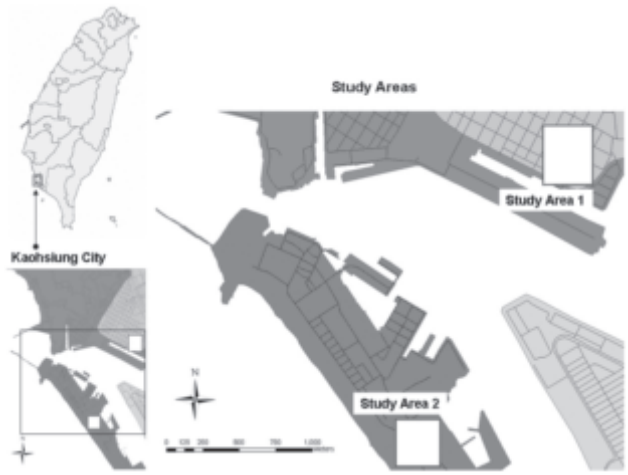

Figure 3. Study areas.

The lidar data were acquired in February 2005 using an Optech ALTM 3070C with a scan interval for each point of approximately 0.7 points/m. A NDSM was derived by subtracting the DEM from the DSM. The NDSM was subsequently resampled to the same grid size as the spatial resolution of the aerial imagery. This study used two types of imagery: a true color image collected simultaneously with lidar data by an Optech ALTM4K02 digital camera with direct exterior orientation parameters and rectified to 0.2 m × 0.2 m grid resolution, and multispectral aerial imagery acquired by a Vexecl UltraCam$_D$ digital camera with 0.09 m ground-sampling distance (GSD) in December 2005, ortho-rectified, and then resampled to a 0.1 m × 0.1 m grid.

Experiment Cases and Discussion

MLC Experiments

In this experiment, the traditional statistic MLC method was used to investigate how lidar data integrated with aerial imagery contributed to urban classification. For the MLC, training samples from four ground categories (i.e., trees, grass, buildings, and roads) were selected on the aerial images and lidar data using ENVI software. Table 3 lists the amount of training data sampled from two study areas. For accuracy assessment, the sizes of randomly sampled test data were determined by Equation 4 (Fitzpatrick-Lins, 1981) as follows:

$$N = \frac{Z^2 (p)(q)}{E^2}, \tag{4}$$

where p is the expected percent accuracy, $q = 100 - p$, E is the allowable error, and $Z = 2$ from the standard normal deviate of 1.96 for the 95 percent two-sided confidence level. However, simple random sampling tends to undersample some small but important areas when using the above equation to determine the sampling size. To ensure that the sampled data were statistically valid, we iteratively applied a random sample method using the sampling size based on Equation 4 until each category accumulated more than 50 samples (Congalton, 1991). Table 3 lists the number of training and test samples for the MLC experiments of the two study areas. Because two different types of aerial imagery were acquired at different times, the number of training and test sites had to be adjusted according to the aerial images used.

Six different combinations of aerial imagery and lidar data were selected to perform MLC. First, two RGB aerial images acquired at different times were used as the standard cases for comparison (cases MLC1 and MLC5 in Table 4). All the additional features described in the experiment results and discussions will refer to these two standard cases. Second, the lidar intensity was added (cases MLC2 and MLC6). Third, the lidar NDSM was added (cases MLC3 and MLC8). Fourth, the lidar intensity and NDSM were added (cases MLC4 and MLC9). Afterward, the NIR band was added to the second RGB image (case MLC7). Finally, the lidar NDSM was added to the MLC7 data set (case MLC10).

Figures 6 and 7 show the MLC resultant images for study areas 1 and 2, respectively. A great deal of noise and numerous speckles are apparent in all the MLC classification results. Figures 6a, 6e, 7a, and 7e illustrate the classification

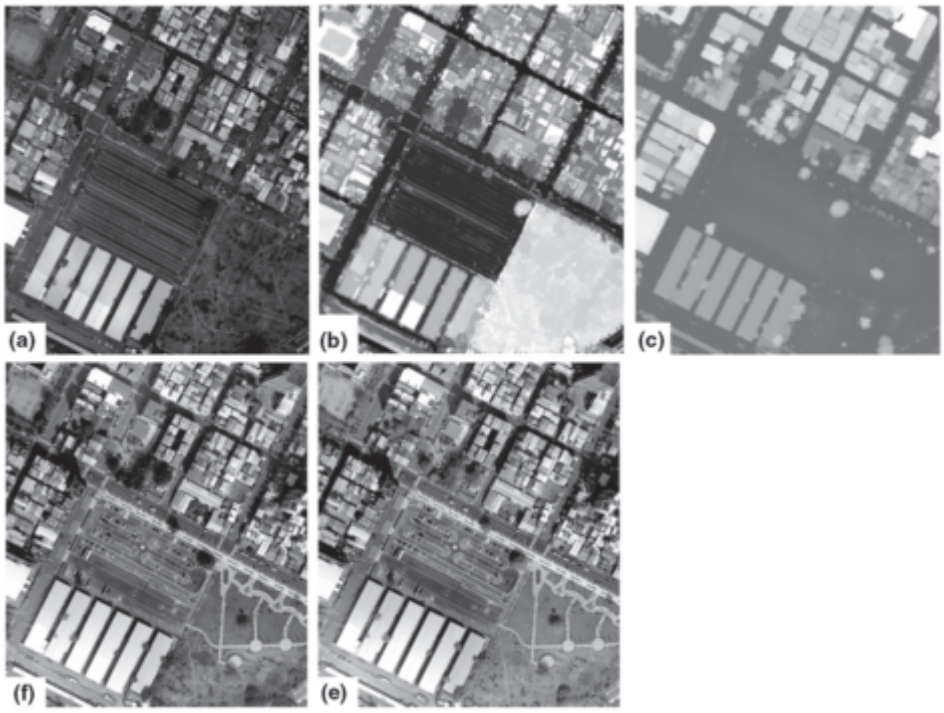

Figure 4. Aerial imagery, lidar intensity, and lidar height raster of study area 1: (a) February 2005 Color Aerial Imagery, (b) February 2005 Lidar Intensity, (c) February 2005 Lidar NDSM, (d) December 2005 Color Aerial Imagery, and (e) December 2005 CIR Aerial Imagery. A color version of this figure is available at the ASPRS website: **www.asprs.org**

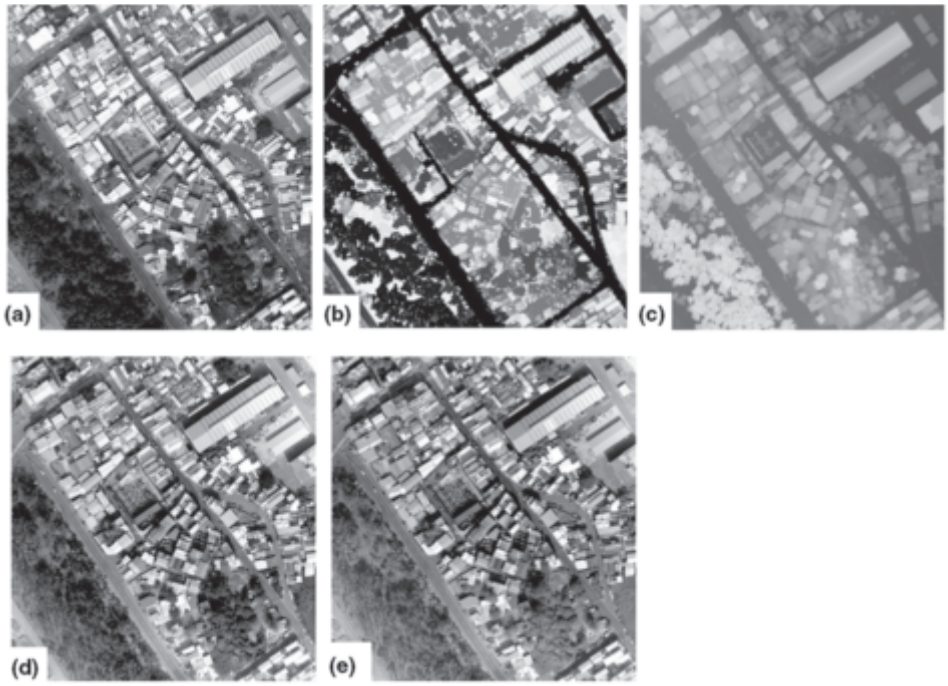

Figure 5. Aerial imagery, lidar intensity, and lidar height raster of study area 2: (a) February 2005 Color Aerial Imagery, (b) February 2005 Lidar Intensity, (c) February 2005 Lidar NDSM, (d) December 2005 Color Aerial Imagery, and (e) December 2005 CIR Aerial Imagery. A color version of this figure is available at the ASPRS website: **www.asprs.org**.

TABLE 3. THE TRAINING DATA AND TESTS USED FOR STUDY AREAS 1 AND 2

			Training Data		Test Data
	Data Set	Category	Pixels	ROIs	Pixels
Study Area1	2005/02 (20cm)	Buildings	482	49	485
		Trees	479	80	73
		Roads	493	27	476
		Grass	497	26	177
	2005/12 (10cm)	Buildings	853	57	482
		Trees	852	84	73
		Roads	834	30	492
		Grass	827	30	164
			Training Data		Test Data
	Data Set	Category	Pixels	ROIs	Pixels
Study Area 2	2005/02 (20cm)	Buildings	551	35	346
		Trees	554	37	189
		Roads	546	21	224
		Grass	549	13	56
	2005/12 (10cm)	Buildings	551	35	346
		Trees	542	36	189
		Roads	546	21	226
		Grass	549	13	54

results for standard cases using RGB aerial imagery. The discrimination confusion between buildings and roads, as well as trees and grass, can be clearly observed from the resultant classification images. This confusion is due to the similar spectral characteristics of these ground objects. After adding the lidar intensity or NIR band, the confusion is still evident in Figures 6b, 7b, 6f, 7f, 6g, and 7g. However, the lidar NDSM resolves the confusion in discrimination, as shown in Figures 6c, 6h, 7c, and 7h. However, incorporation with height information caused some shadows between buildings in the narrow lanes to be misclassified as trees, as is evident from Figures 6c, 6h, 7c, and 7h. Figures 6d, 6i, 7d, and 7i show that integrating lidar intensity and NDSM with the RGB aerial imagery did not improve the classification result significantly. Finally, when integrating the NIR imagery and the lidar NDSM, the false discrimination of shadows was removed because of the good vegetation-discrimination capability of the NIR band. This is shown in Figures 6j and 7j.

Table 4 lists the accuracy assessment results for all the MLC experiments. Generally, the overall accuracy and Kappa index values of the equivalent cases (e.g., MLC1 versus MLC5, MLC2 versus MLC6, and MLC3 versus MLC8) using the data set acquired in February 2005 were 5 to 10 percent higher than those using the data set acquired in December 2005. This difference mainly reflected the temporal inconsistencies between lidar data and aerial imagery. The overall accuracy of the two standard RGB imagery experiments (cases MLC1 and MLC5) only ranged from 60 to 70 percent, which is not satisfactory for urban classification applications. The overall accuracy improved by approximately 3 to 7 percent when adding lidar intensity (cases MLC2 and MLC6) and 3 to 10 percent when adding the NIR band (case MLC7) to the RGB imagery. Adding lidar NDSM (cases MLC3 and MLC8) improved the overall accuracy by about 12 to 18 percent, which was more significant than adding lidar intensity and the NIR band. Adding both the NIR and the lidar NDSM into RGB imagery (case MLC10) improved the overall accuracy by 14 to 18 percent more than adding the NIR band (case MLC7) and 5 to 12 percent more than adding the NDSM (case MLC8). The integration of NIR and lidar NDSM with RGB imagery resulted in 4 percent greater accuracy than the case without NIR (case MLC3) in study area 2. However, this was not true in study area 1 because trees were rare and temporal inconsistency existed between the two standard case images. The contribution of lidar height to urban-feature classification was thus confirmed in this study not only by visually checking classification images but also by accuracy assessment.

The OBC and KBCS Experiments

OBC and KBCS were performed for the two study areas to investigate KBCS performance. The feature vectors used for this experiment were NDSM, penetrability, smoothness, ND, AIS, lidar intensity, NDVI, and lidar-TVI calculated by applying the RDM and the IVDM to lidar data and aerial imagery. The first five features are derived by lidar height, while the other three are spectral-based. These features can be calculated by most commercial remote sensing image processing tools or by common programming language.

The OBC experiment was performed using Definiens Imaging's eCognition® software in two stages: image network segmentation followed by supervised nearest-neighbor classification (Baatz *et al.*, 2004). First, we assigned a higher weight value for the lidar NDSM because of its higher homogeneity in the gray level; we assigned lower weight values or zero for lidar intensity, NDVI, and lidar-TVI. The penetrability, smoothness, ND, and AIS were set to zero because of their large height gradients at building boundaries, which may degrade the segmentation results. Next, we specified the size and homogeneity criteria for ground objects. These two criteria were determined by selecting the scale parameter, color, shape, smoothness, and compactness. By visually interpreting segmentation results from different images, we chose a set of segmentation parameters to create a network of image objects for study areas 1 and 2. Afterward, the training samples could be collected from the segmented objects. In the classification stage, spectral nearest-neighbor classification was performed to classify the ground features into four categories. The classification accuracy was evaluated using test data sampled from December 2005 images, as for the test data used in cases MLC5 to MLC10.

The KBCS classification was performed using programs written in Matlab. Thresholds set from expert experience, such as the lowest building height, the smallest building block area, and two thresholds for lidar intensity, were entered into rules of the knowledge base after examining the lidar data and aerial imagery of the study areas. The rest of the thresholds were set as default values (see Table 1) for most of the time, especially during the first test. After investigating the initial result of the KBCS classification, we adjusted some of the threshold values. Finally, thresholds of the KBC were set according to specific requirements. In addition to the KBC thresholds, the boundaries of areas with temporal inconsistency were digitized using GIS software according to the aerial imagery of December. Then these features were used to create the temporal mask. For example, the newer imagery revealed that two trees had been cut down. Lidar height was used to extract the shape of the trees to build the temporal mask. The output of the KBCS was stored in the ENVI native image format. The same accuracy evaluation was then performed using the same test data sets used for the OBC experiments.

Figure 8 shows the resultant classification images from the OBC (Figures 8a and 8c) and the KBCS (Figures 8b and 8d) experiments in study areas 1 and 2, respectively. The OBC and KBCS classified images have superior visual interpretability compared to the MLC classified image (case MLC10 in Figures 6j and 7j); however, some differences exist between the OBC and KBCS classifications. In the OBC experiment, the segmentation parameters were chosen from

TABLE 4. ACCURACY ASSESSMENTS OF FOUR MLC, OBC, AND KBCS EXPERIMENTS

Experiment 1		OA	KI	Producer's Accuracy (%)				User's Accuracy (%)			
				Bd	Tr	Rd	Gs	Bd	Tr	Rd	Gs
	MLC1	69.36	0.5483	65.15	58.90	72.27	77.40	81.03	29.45	67.45	83.03
	MLC2	76.38	0.6475	83.30	63.01	68.07	85.31	75.23	37.40	82.86	94.38
	MLC3	87.12	0.8075	90.31	73.97	85.71	87.57	88.48	49.09	94.01	90.12
	MLC4	84.97	0.7761	92.16	78.08	76.47	90.96	81.13	49.14	98.64	92.00
Study	MLC5	64.16	0.4660	57.47	60.27	72.56	60.37	73.87	28.76	65.63	71.22
Area 1	MLC6	66.80	0.5090	62.66	67.12	71.14	65.85	71.06	26.78	72.61	90.00
	MLC7	67.30	0.5055	62.86	67.12	73.78	60.98	73.90	37.98	66.36	80.00
	MLC8	76.38	0.6537	82.37	79.45	75.00	61.59	82.02	29.74	92.02	77.10
	MLC9	77.37	0.6661	82.16	78.08	77.64	62.20	79.36	29.53	94.09	91.07
	MLC10	81.58	0.7214	94.40	75.34	76.63	61.59	81.54	42.64	93.09	84.87
	MLC1	70.06	0.5723	67.92	77.25	73.21	46.43	81.88	79.78	59.85	36.62
	MLC2	75.95	0.6482	80.35	86.24	59.38	80.36	75.96	76.89	73.89	78.95
	MLC3	84.05	0.7673	84.39	87.30	86.16	62.50	88.48	89.19	75.39	79.55
	MLC4	84.29	0.7676	93.06	89.95	68.30	75.00	81.11	83.74	93.29	82.35
Study	MLC5	60.00	0.4423	57.23	67.72	60.62	48.15	86.09	53.78	52.90	29.55
Area 2	MLC6	64.42	0.4940	64.74	81.48	50.88	59.26	78.05	46.81	79.31	59.26
	MLC7	70.55	0.5750	69.08	79.37	71.24	46.30	79.14	78.13	60.30	46.30
	MLC8	76.56	0.6605	80.92	79.37	70.35	64.81	81.87	65.22	88.83	54.69
	MLC9	76.20	0.6484	84.68	82.01	60.62	66.67	74.74	64.85	99.28	78.26
	MLC10	88.34	0.8270	98.27	85.19	76.55	85.19	83.13	94.71	98.30	76.67

Experiment 2		OA	KI	Producer's Accuracy (%)				User's Accuracy (%)			
				Bd	Tr	Rd	Gs	Bd	Tr	Rd	Gs
	OBC	88.05	0.8203	83.44	62.96	95.69	92.18	98.79	72.86	82.07	87.30
	OBC2	90.35	0.8535	93.66	64.20	95.69	79.33	96.42	75.36	87.06	89.87
Study	KBCS	93.90	0.9062	95.89	65.82	96.15	94.81	98.11	89.66	92.40	87.95
Area 1	KBCS1	80.71	0.7182	93.66	64.20	81.47	50.84	96.42	75.36	84.00	92.86
	KBCS2	87.06	0.8004	93.66	64.20	96.77	54.19	96.42	75.36	80.18	89.81
	KBCS3	92.91	0.8938	94.89	66.67	93.10	98.88	97.27	76.06	94.12	85.92
	OBC	86.40	0.8026	86.99	87.83	87.61	72.73	93.19	79.81	84.26	80.00
	OBC2	89.22	0.8420	91.33	78.84	94.69	89.09	88.76	95.51	87.35	83.05
Study	KBCS	93.87	0.9111	92.49	92.06	97.79	92.73	97.26	98.31	88.40	85.00
Area 2	KBCS1	76.20	0.6722	91.04	76.19	52.44	80.00	88.24	97.30	96.72	81.48
	KBCS2	88.47	0.8313	91.04	76.19	94.22	90.91	88.24	97.30	86.89	75.76
	KBCS3	92.16	0.8868	90.17	93.65	93.81	92.73	97.50	91.71	89.08	78.46

Note:
MLC1–4 using 2005/02 aerial imagery
MLC1: RGB
MLC2: RGB + Lidar Intensity
MLC3: RGB + nDSM
MLC4: RGB + Lidar Intensity + nDSM
MLC5–10 using 2005/12 aerial imagery
MLC5: RGB
MLC6: RGB + Lidar Intensity
MLC7: RGB + NIR
MLC8: RGB + nDSM
MLC9: RGB + Lidar Intensity + nDSM
MLC10: RGB + NIR + nDSM
OBC: Image Segmentation + Nearest Neighbor Classification
OBC2: Image Segmentation + KBCS rules
KBCS: Knowledge-Based Classification System
KBCS1: One-Level Scheme KBCS
KBCS2: Two-Level Scheme KBCS
KBCS3: KBCS without KBC
OA: Overall Accuracy (%)
KI: Kappa Index
Bd: Buildings
Tr: Trees
Rd: Roads
Gs: Grass

some experiments based on visual interpretation of the segmentation results. Larger segmentation parameters were used for the OBC for study area 1, generating larger segmented images. Therefore, it was difficult to discriminate small objects, such as small trees around a large grassy field and pavement inside the grassy field. Another problem related to the OBC segmentation parameters was that the edges of the buildings were not as straight as those for the KBCS. In contrast, the smaller segmentation scale parameter of the OBC for study area 2 could identify narrow lanes and smaller building blocks. The smaller-scale parameter produced straight edges for most of the buildings and derived a much smaller misclassified segmentation than in study area 1. Table 4 shows the accuracy assessment results for the OBC and KBCS, indicating greater overall accuracy and Kappa index values for the KBCS than for the OBC.

One additional OBC experiment was performed to evaluate the improvement when knowledge-based rules were applied to the OBC (case OBC2). Setting the OBC scale parameter to 1 created very small segmented images. Then, the KBCS rules were applied to each of the segmented features. As shown in Table 4, the overall accuracy of OBC2 did improve by about 2 percent for both study areas, indicating that the knowledge-based approach can improve the performance of the OBC.

Three additional KBCS experiments were conducted to evaluate the KBCS performance. First, two additional KBCS experiments (KBCS1 and KBCS2) were implemented by

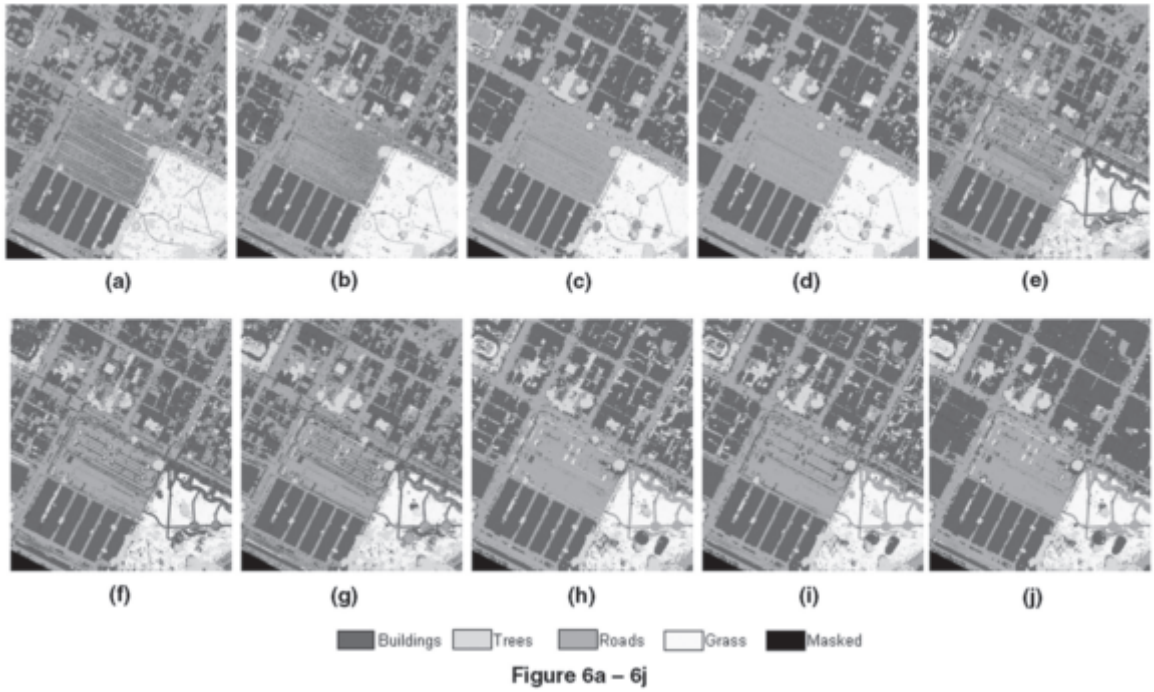

Figure 6. MLC experiment resultant images of study area 1: (a) MLC1, (b) MLC2, (c) MLC3, (d) MLC4, (e) MLC5, (f) MLC6, (g) MLC7, (h) MLC8, (i) MLC9, and (j) MLC10. A color version of this figure is available at the ASPRS website: **www.asprs.org**.

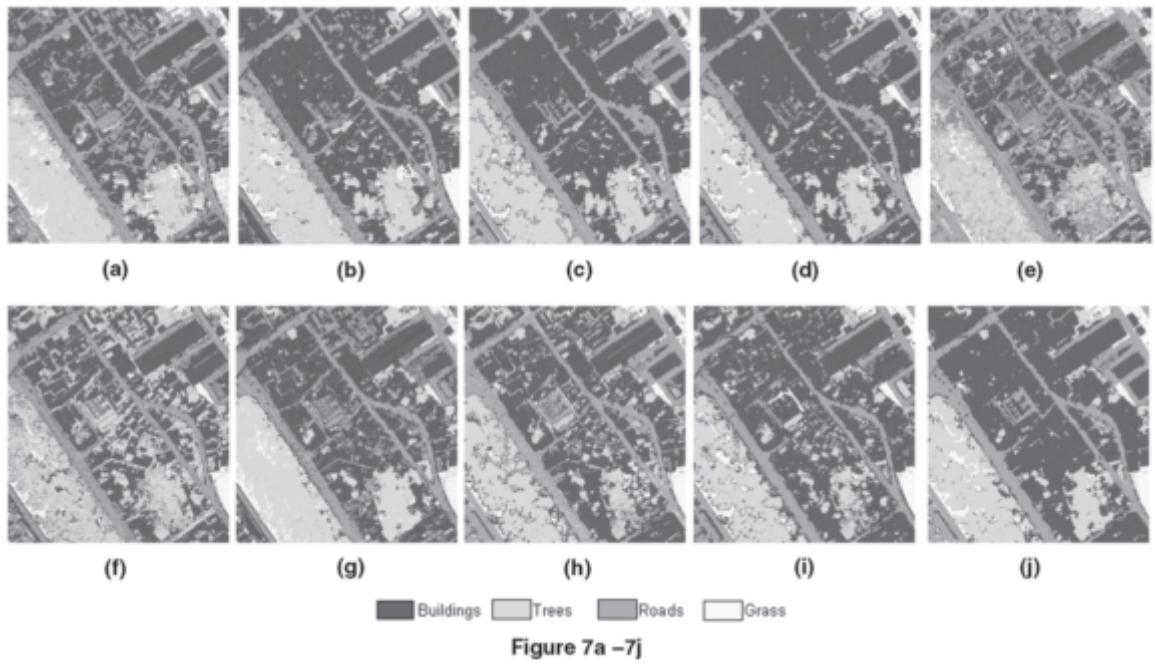

Figure 7. MLC experiment resultant images of study area 2: (a) MLC1, (b) MLC2, (c) MLC3, (d) MLC4, (e) MLC5, (f) MLC6, (g) MLC7, (h) MLC8, (i) MLC9, and (j) MLC10. A color version of this figure is available at the ASPRS website: **www.asprs.org**.

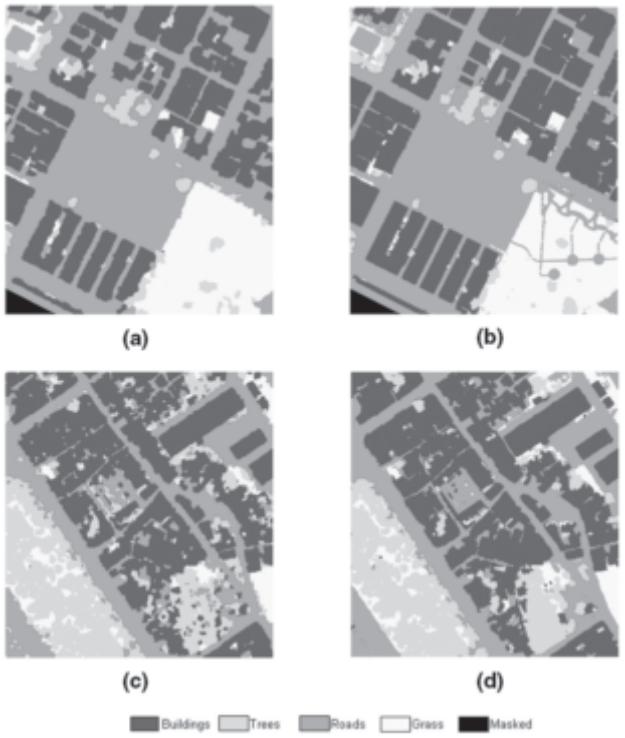

Figure 8. (a) OBC, and (b) KBCS resultant images for study area 1; (c) OBC, and (d) KBCS resultant images for study area 2. A color version of this figure is available at the ASPRS website: **www.asprs.org**.

reducing the three-level scheme to one-level and two-level schemes. The one-level scheme applied all the rules at one level. The two-level scheme merged low-height and mid-height levels together to simplify the three-level scheme. Finally, the three-level scheme was used but without the application of any KBC rules (KBCS3). Table 4 lists the results of the accuracy assessment.

Generally, except for the KBCS, no vertical layer scheme exists for either the pixel-based or the OBC approach. The advantage of the new three-height-level classification framework is that it offers a mechanism not only to reduce the number of categories at each level, but also to overcome the ambiguity between high- and low-height objects. Based on this design, the categories at the low-height level are roads and grass, while only buildings and trees need to be classified at the high-height level. The most complex ground objects in the mid-height level are separated before classification to overcome the discrimination difficulty caused by these objects. The results of additional KBCS experiments (KBCS1 and KBCS2) indicate that two-level and three-level schemes improve the overall accuracy up to 12 and 17 percent, respectively, over a one-level scheme. The major improvement derives from enhanced accuracy of roads and grass, demonstrating that the role of the mid-height level is to resolve the ambiguity of small objects on the roads and grass. The accuracy improvement may increase as the number of levels increases; however, the complexity of classification rules may also increase simultaneously.

Our findings show that residual information produced by noise-removal procedures in rule-based classification or unclassified classes is well modeled and adjusted by KBC. Images adjusted by KBC were refined without the speckles usually seen in the results of most pixel-based classification methods. The rules used by the proposed KBC are stored in the knowledge base, which means that they are a part of the KBCS. In addition, the KBC rules are set up according to expert knowledge. This knowledge was used to adjust the four categories one by one, considering small and long-shaped segments caused by noise and shadows. The KBCS including KBC showed 1.0 and 1.7 percent improvements for study areas 1 and 2, respectively, in overall accuracy compared to the KBCS without KBC (KBCS3).

Several advantages exist to using the proposed knowledge-based classification system to separate ground features into categories. The resultant KBCS images are clean and contain less noise and fewer speckles. The knowledge-based method is also quite understandable and flexible. New rules can be added to the knowledge base to increase the classification ability. This paper defines the types of knowledge needed for ground-feature discrimination and describes how to extract that knowledge from lidar data and aerial imagery, determine the thresholds for KBCS, and apply these classification rules to build an expert system for performing ground-object classification over complex urban areas.

Conclusions

While the spatial resolution of remotely sensed data has improved, multispectral images are insufficient for urban classification due to confusion in discriminating between trees and grass, misclassification of buildings caused by diverse roof compositions and shadow effects, and difficulty in distinguishing cars on roads. The results of MLC experiments indicate that classification accuracy is not satisfactory in standard cases involving RGB aerial imagery or even NIR imagery. However, the incorporation of lidar data, especially NDSMs, significantly improves accuracy. Thus, urban classification is highly dependent on lidar height rather than on NIR imagery.

Our proposed knowledge-based classification rules improved urban classification performance. Three factors may explain the success of this method. First, the new three-height-level classification framework not only reduces the number of categories at each level but also overcomes the ambiguity between high-height and low-height objects. In addition, the A–V–N principle further simplifies urban classification at each level, and the KBC successfully removes shadows between buildings from the preliminary classified image. The OBC and KBCS experiment results indicate that the overall accuracy of the KBCS is 6 to 7 percent better than that of the OBC approach. Moreover, the visual details in the KBCS are superior to those of the OBC without involving a selection procedure for optimal segmentation parameters.

The proposed KBCS provides the procedures and mechanisms to formalize knowledge into classification rules. The advantage of the KBCS is that its procedure can be repeated by designing a stand-alone program or applying the rules to commercial classification software with "expert system" functionality, such as eCognition® or ERDAS Imagine®. In the future, more subcategories can be extended to the KBCS according to user requirements. More ground-feature discriminative models and inference rules should be explored if more subcategories are needed.

Acknowledgments

The authors sincerely acknowledge the three anonymous reviewers for their helpful comments and suggestions. This research was supported by Asian Pacific Ocean Research

Center, National Sun Yat-sen University and National Science Council, Republic of China with Grant 94–2611-E-110–007. We also want to greatly appreciate Chung Hsing Surveying Co., LTD for providing the lidar data and aerial imagery.

References

Arefi H., M. Hahn, and J. Lindenberger, 2003. Lidar data classification with remote sensing tools, *Proceedings of the ISPRS Commission IV Joint Workshop: Challenges in Geospatial Analysis, Integration and Visualization II*, 08–09 September, Stuttgart, Germany, pp. 131–136.

Baatz, M., U. Benz, S. Dehghani, and M. Heynen, 2004. *eCognition User Guide 4*, Definiens Imagine GmbH, Munchen, Germany.

Baltsavias, P.E., and A. Gruen, 2003. A comparison of aerial photos, lidar and IKONOS for monitoring cities, *Remotely Sensed Cities* (V. Mesev, editor), Taylor & Francis, New York, pp. 47–84.

Congalton, R.G., 1991. A review of assessing the accuracy of classifications of remotely sensed data, *Remote Sensing of Environment*, 37(1):35–46.

Deering, D.W., J.W. Rouse, R.H. Haas, and J.A. Schell, 1975. Measuring forage production of grazing units from Landsat MSS data, *Proceedings of the 10th* International Symposium on Remote Sensing of Environment, ERIM 2, pp. 1169–1178.

Elberink, S.O., and H.G. Maas, 2000. The use of anisotropic height texture measurements for the segmentation of airborne laser scanner data, *International Archives of Photogrammetry and Remote Sensing*, Amsterdam, XXXIII(B3):678–684.

Fitzpatrick-Lins, K., 1981. Comparison of sampling procedures and data analysis for a land-use and land-cover map, *Photogrammetric Engineering & Remote Sensing*, 47(3):343–351.

Giarratano, J., and G. Riley, 1989. *Expert Systems: Principles and Programming*, PWS-KENT Publishing Company, Boston, 632 p.

Haala, N., and C. Brenner, 1999. Extraction of buildings and trees in urban environment, *ISPRS Journal of Photogrammetry and Remote Sensing*, 54(2–3):130–137.

Hill, A.R., G.M. Smith, R.M. Fuller, and N. Veitch, 2002. Landscape modelling using integrated airborne multispectral and laser scanning data, *International Journal of Remote Sensing*, 23(11):2327–2334.

Hodgson, E.M., J.R. Jensen, J.A. Tullis, K.D. Riordan, and C.M. Archer, 2003. Synergistic use of lidar and color aerial photography for mapping urban parcel imperviousness, *Photogrammetric Engineering & Remote Sensing*, 69(9):973–980.

Hu, Y., and V. Tao, 2005. Hierarchical recovery of digital terrain models from single and multiple return lidar data, *Photogrammetric Engineering & Remote Sensing*, 71(4):425–434.

Huang, M.J., S.W. Shyue, and L.W. Lee, 2006. Update urban GIS data by feature extraction from lidar data and aerial digital color imagery, *Proceedings of the Sixth International Conference on ASIA GIS (ASIA GIS 2006)*, Malaysia, March.

Hung, M.-C., and M.K. Ridd. 2002. A sub-pixel classifier for urban land-cover mapping based on a maximum likelihood approach and expert system rules, *Photogrammetric Engineering & Remote Sensing*, 68(11):1173–1180.

Liu, X.H., A.K. Skidmore, and H.V. Oosten, 2002. Integration of classification methods for improvement of land-cover map accuracy, *ISPRS Journal of Photogrammetry & Remote Sensing*, 56(4):257–268.

Ma, R., 2005. DEM generation and building detection from lidar data, *Photogrammetric Engineering & Remote Sensing*, 71(7):847–854.

Nagao, M., and T. Matsuyama, 1980. *A Structural Analysis of Complex Aerial of Photographs*, Plenum Press, New York.

Ostu, N., 1979. A threshold selection method from gray-level histograms, *IEEE Transactions on Systems, Man, and Cyernetices*, SMC-9(1):62–66.

Repaka, R.S., D. Truax, E. Kolstad, and C. Hara, 2004. Comparing spectral and object based approaches for classification and transportation feature extraction from high resolution multispectral imagery, *Proceedings of the ASPRS Annual Conference*, 23–28 May, Denver, Colorado, pp. 204–215.

Richards, J.A., and X. Jia, 1999, *Remote Sensing Digital Image Analysis*, Springer-Verlag, Berlin, 363 p.

Ridd, M.K., 1995. Exploring a V-I-S (Vegetation-Impervious Surface-Soil) model for urban ecosystem analysis through remote sensing: Comparative anatomy for cities, *International Journal of Remote Sensing*, 16(12):2165–2185.

Rottensteiner, F., J. Trinder, S. Clode, and K. Kubik, 2005. Using the Dempster-Shafer method for the fusion of lidar data and multispectral images for building detection, *Information Fusion*, 6(4):282–300.

Stefanov, W.L., M.S. Ramsey, and P.R. Christensen, 2001. Monitoring urban land-cover change: An expert system approach to land-cover classification of semiarid to arid urban centers, *Remote Sensing of Environment*, 77(2):173–185

Taubenböck, H., T. Esch, and A. Roth, 2006. An urban classification approach based on an object-oriented analysis of high resolution satellite imagery for a spatial structuring within urban areas, *Proceedings of the 1st EARSeL Workshop of the SIG Urban Remote Sensing Humboldt-Universität zu Berlin*, 02–03 March.

Ton, J., J. Sticklen, and A.K. Jain, 1991. Knowledge-based segmentation of Landsat images. *IEEE Transactions on Geosciences and Remote Sensing*, 29(2):222–232.

(Received 29 March 2007; accepted 20 April 2007; revised 14 May 2007)